Sensorless adaptive optics system based on image second moment measurements

Agbana, Tope; Yang, H.; Soloviev, Oleg; Vdovine, Gleb; Verhaegen, Michel

DOI
10.1117/12.2227551

Publication date
2016

Document Version
Final published version

Published in
Proceedings of SPIE

Citation (APA)
Agbana, T., Yang, H., Soloviev, O., Vdovine, G., & Verhaegen, M. (2016). Sensorless adaptive optics system based on image second moment measurements. In P. Schelkens, T. Ebrahimi, G. Cristóbal, F. Truchetet, & P. Saarikko (Eds.), *Proceedings of SPIE: Optics, Photonics and Digital Technologies for Imaging Applications IV* (Vol. 9896). Article 989609 (Proceedings of SPIE; Vol. 9896). SPIE. https://doi.org/10.1117/12.2227551

Sensorless Adaptive Optics System based on Image Second Moment Measurements

Temitope E. Agbana[a], Huizhen Yang[b], Oleg Soloviev[a,c,d], Gleb Vdovin[a,c,d], and Michel Verhaegen[a]

[a]Delft Center for System and Control, Delft University of Technology, Mekelweg 2, 2628 CD,Delft, the Netherlands
[b]Department of Electronic Engineering, Huaihai Institute of Technology, Lianyungang, Jiangsu 222005, China
[c]Flexible Optical. B.V., Polakweg 10-11, 2288 GG Rijswijk ZH, the Netherlands
[d]ITMO University,Kronverksy pr. 49, St. Petersburg, Russia

ABSTRACT

This paper presents experimental results of a static aberration control algorithm based on the linear relation between mean square of the aberration gradient and the second moment of point spread function for the generation of control signal input for a deformable mirror (DM). Results presented in the work of Yang *et al.*[1] suggested a good feasibility of the method for correction of static aberration for point and extended sources. However, a practical realisation of the algorithm has not been demonstrated. The goal of this article is to check the method experimentally in the real conditions of the present noise, finite dynamic range of the imaging camera, and system misalignments. The experiments have shown strong dependence of the linearity of the relationship on image noise and overall image intensity, which depends on the aberration level. Also, the restoration capability and the rate of convergence of the AO system for aberrations generated by the deformable mirror are experimentally investigated. The presented approach as well as the experimental results finds practical application in compensation of static aberration in adaptive microscopic imaging system.

Keywords: wavefront sensorless adaptive optics, experimental results, static aberration,microscopic imaging system

1. INTRODUCTION

AO systems without the wavefront sensor are used in several applications like microscopy, laser intra-cavity aberration corrections, optical tweezers, free space optics communications, power delivery. Mostly they are based on a global non-linear optimisation of some performance metrics calculated from the intensity distribution in the focal plane.[2] These methods are usually iterative and require a lot of intensity measurements. Realizing a wavefront sensorless (WFSless) adaptive optics (AO) systems which features faster convergence with minimal photodetector measurement is of great potential in both static and dynamic wavefront correction fields,[3,4] so a number of methods have used model-based approach with linearisation of the metrics for small aberrations.[5–7] Booth[8] proposed to use the second moment of PSF for wavefront sensorless control in AO for large aberration, using Lukosz–Zernike functions for control. Linhai and Rao[9] extended the method to a generalized model-based control, insensitive to the selection of sets of functions and their bias values. Yang *et al.*[1] in their work developed the second moment-based method further for the aberration correction for the imaging of extended sources.

Results of reference 1 suggested a good feasibility of the method for correction of static aberration, both for the point and extended sources. However, a practical realisation of this algorithm has not been demonstrated. The goal of this article is to check the method experimentally in the real conditions of the present noise, finite dynamic range of the imager, and system misalignments. Furthermore, the performance of the proposed

Further author information: (Send correspondence to Temitope E. Agbana)
Temitope E. Agbana: E-mail: t.e.agbana@tudelft.nl, Telephone: +3152785305

Optics, Photonics and Digital Technologies for Imaging Applications IV, edited by Peter Schelkens, Touradj Ebrahimi, Gabriel Cristóbal, Frédéric Truchetet, Pasi Saarikko, Proc. of SPIE Vol. 9896, 989609 · © 2016 SPIE · CCC code: 0277-786X/16/$18 · doi: 10.1117/12.2227551

algorithm is experimentally compared to an optimisation algorithm such as the Stochastic Parallel Gradient Descent SPGD algorithm.[10,11]

This paper presents experimental results of a fast control algorithm, which is based on linear relation between mean square of the aberration gradients and second moment of the image intensity distribution for generation of control signal input to the actuators of the deformable mirror (DM).

This paper is organised as follows: in Section 2, a summarised theoretical framework of the control algorithm based on reference 1, is presented. Section 3 describes the design of the wavefront sensorless adaptive optics imaging system and presents the experimental results obtained in the setup.

2. THEORETICAL FRAMEWORK OF CONTROL ALGORITHM

Based on physical optics, a linear relationship between the second moment of the intensity distribution and the mean-square gradient magnitude of the wavefront aberration has been established in reference 1. A mathematical expression of this relationship is summarised in the following equations:

$$\mathrm{SM} = \mathrm{SM}_0 - c_0(R) \int_{R^2} ((P(x,y)\phi'_x(x,y)))^2 dxdy. \tag{1}$$

SM represents the second moment computed from the focal plane intensity distribution, SM_0 is the second moment of the wavefront aberration to be corrected, c_0 is a constant representing the slope, $c_0 = \frac{1}{4\pi^2}$. $P(x,y)$ is the unaberrated pupil function, $\phi(x,y)$ is the pupil aberration and (x,y) are the pupil coordinates expressed in wavelength. Central second moment is used here since we have excluded the influence of tip and tilt in this experimental validation. The SM is defined as :

$$\mathrm{SM} = \frac{\iint_D ((x-x_0)^2 + (y-y_0)^2) \cdot I(x,y) \mathrm{d}x\mathrm{d}y}{\int I(x,y) \mathrm{d}x\mathrm{d}y}, \tag{2}$$

where $I(x,y)$ is the far field intensity distribution, and

$$x_0 = \frac{\sum_{x,y} x \cdot I(x,y)}{\sum_{x,y} I(x,y)}, \quad y_0 = \frac{\sum_{x,y} y \cdot I(x,y)}{\sum_{x,y} I(x,y)}.$$

To estimate the control signal of the deformable mirror, the measured mirror influence function $\psi_i(x,y)$ are taken as predetermined basis function shape of the mirror. The basis function shape with coefficient β is sequentially added to the wavefront to be corrected. The detection measurements are recorded and N second moments SM_i $(i = 1, \ldots, N)$ are computed according to equation (2). The control parameter V can be calculated as

$$V = \frac{S^{-1} c_0 M}{2\beta} - \frac{\beta S^{-1} S_m}{2}, \tag{3}$$

where

$$M \equiv \begin{bmatrix} \mathrm{SM}_1 - \mathrm{SM}_0 \\ \mathrm{SM}_2 - \mathrm{SM}_0 \\ \mathrm{SM}_3 - \mathrm{SM}_0 \\ \vdots \\ \mathrm{SM}_N - \mathrm{SM}_0 \end{bmatrix}, \tag{4}$$

S is the matrix representing the mean square gradient of the aberration wavefront which can be predetermined from the measured influence function of the deformable mirror, D is the area of the pupil. Given the measured influence function $\psi_i(x,y)$, S can be evaluated as

$$S(i,j) = D^{-1} \iint_D \left[\frac{\partial}{\partial x}\psi_i(x,y) \cdot \frac{\partial}{\partial x}\psi_j(x,y) + \frac{\partial}{\partial y}\psi_i(x,y) \cdot \frac{\partial}{\partial y}\psi_j(x,y) \right] \mathrm{d}x\mathrm{d}y \tag{5}$$

The control algorithm is hence subdivided into 2 parts: (a) The preprocessing step where S and S_m (diagonal vector of S) and S^{-1} (inverse matrix) are computed based on the measured influence function of the DM and (b) The iteration step where the aberration is being corrected.

3. MODEL-BASED WAVEFRONT SENSORLESS AO SYSTEM: EXPERIMENTAL SET-UP AND VALIDATION

We have used the following experimental set up (see Fig.1). The light source is a single mode fibre coupled laser (Thorlabs S1FC635) with a wavelength of 635 NM. The light cone exiting the source is limited by an iris placed $100mm$ from the point source. A collimating lens L_1 with focal length of 200 mm is used to collimate the light exiting the iris. Two achromatic doublets L_2 and L_3, with focal lengths of 150 mm and 100 mm respectively, rescale the incoming light into a 10 mm beam over a 15 mm diameter area of the Micromachined Membrane Deformable Mirror (MMDM). The MMDM is a low-order mirror (OKO Technologies, the Netherlands) with 17 actuators and built-in tip-tilt stage; the mirror has maximum stroke of 9.4 μm. The computer interface provides 8-bit voltage control for the output channels and an high voltage amplifier produces the final desired voltage (in the range of $0 \ldots 255$ V to each actuator. The reflected light from the MMDM is spilt into two arms: the calibration arm and the observation arm (focal plane).

The calibration arm is used only once in the beginning of the experiment for the purpose of measuring the influence functions of the actuators of the MMDM (see Section 3.2), and is not used in the main algorithm. Another pair of achromatic doubles L_5 and L_6,with focal lengths of 250 mm and 75 mm respectively, conjugates and rescales the MMDM plane on the Shack-Hartmann Wavefront Sensor (SHWFS). The SHWFS has a microlens array (300×300 lenslets) with a pitch of 192 μm and focal length of 3.87 mm. The wavefront is measured at maximum rate of 12.55 Hz. The diameter of the wavefront on the MMDM is 10 mm, after conjugation on the sensor through the lenses L_5 and L_6, the pupil radius becomes $r_{\text{pupil}} = 3.0$ mm. This pupil radius is used for the measurement of the influence function used as the basis function in this model.

The second arm consist of a focusing lens with focal length of 500 mm and an imaging camera (Thorlabs DCC1545M) which registers the intensity distribution of the point source at the focal plane.

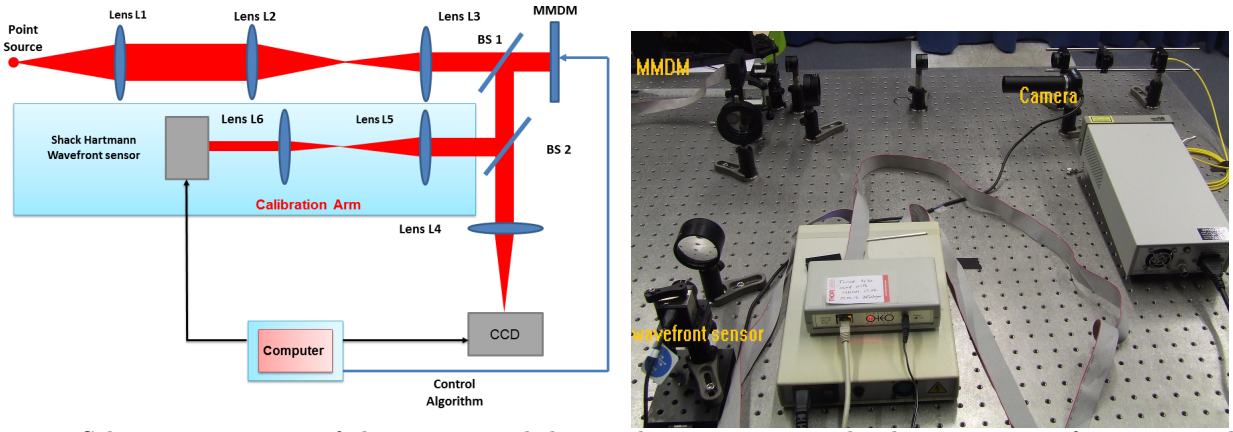

Figure 1: Schematic overview of the set-up used during the experiment. The design consist of two arms: the calibration arm which is used only for the measurement of the influence functions of the actuators of the MMDM and the observation arm, where the focal intensity distribution of the point source is registered on the science camera.

3.1 Measuring the performance limits of the actuators

As a first test of the setup, we have done a simple experiment that doesn't require the knowledge of the response functions and also tests the performance limit of the actuators of the MMDM with respect to the measurement of the second moment of the intensity distribution. In the experiment, we checked the change of the second moment of the PSF with linear change of each of the control signal coordinate. For an unknown static aberration ϕ_0, the aberration superimposed by poking actuator i is represented as:

$$\phi_\alpha = \phi_0 + \alpha\psi_i, \quad \alpha \in [-1, 1]. \tag{6}$$

As previously established, the relationship between the second moment of the intensity distribution and the MSG of the aberration is mathematically expressed as:

$$\mathrm{SM}(\alpha) \propto \frac{1}{4\pi^2} \int P^2(x) \left|\nabla \phi_\alpha\right|^2 \mathrm{d}x \tag{7}$$

Substituting equation (6) into equation (7), with $P(x) = 1$ inside the aperture and $P(x) = 0$ otside of it, we have:

$$\mathrm{SM}(\alpha) \propto \frac{1}{4\pi^2} \int \left(\left|\nabla \phi_0\right|^2 + 2\alpha(\nabla \psi_i, \nabla \phi_0) + \alpha^2 (\nabla \psi_i)^2 \right) \mathrm{d}x \tag{8}$$

From equation (7) it can be inferred that the poking of each actuator using a discrete control signal $\alpha \in [-1, 1]$ yields a parabolic response of its second moment of the intensity measurement at the focal plane. This was done experimentally in the following proceedings: a discrete control signals $\alpha \in [-1, 1]$ was applied to a selected actuator while a constant bias control signal $\boldsymbol{\alpha}^0$ was giving to all other actuators. For each value of the control signal, the intensity distribution was recorded by the CCD and the second moment was computed accordingly. The computed SM was plotted against the signal α. The examples of the resulting plots for two of the mirror actuators are presented in Fig. 2. The experimental result confirms the mathematical solution obtained. As shown in the plotted image, the actuator reaches its performance limit when the control signal exceeds 0.931. Based on this measurement result, the actuator control signal was set to operate in the range $[-0.931, 0.931]$.

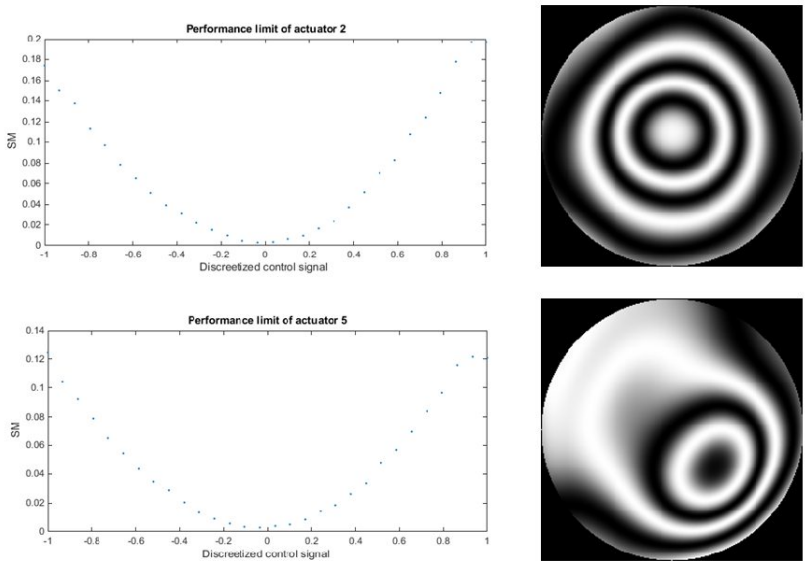

Figure 2: Performance limit of the actuator with respect to the second moment of measured intensity distribution. The plots of the SM against control signal for actuator 2 and 5 are plotted. The interferogram of the corresponding influence function is also shown.

3.2 Influence function measurement

Before the first use, the system should be calibrated: one needs to know the gradients of the influence functions of the mirror used in the phase model:

$$\phi = \sum_{i=1}^{N} r_i \psi_i, \tag{9}$$

where ϕ is the phase aberration formed by the surface of the mirror, N is the number of actuators, r_i is the control signal for the i^{th} actuator, $r_i \in [-1, 1]$, and ψ_i is the corresponding measured influence function. The influence functions are the responses of the mirror membrane to the action of one particular isolated actuator. The set of function obtained is grouped into a matrix called the influence functions matrix.

To measure the influence function we proceeded in the following steps:

1. A random search (non-classical) iterative optimisation algorithm was used to control the MMDM shape to maximise the intensity (performance metric) of the point spread function (PSF) registered by the CCD at the focal plane. As a result of this optimisation, the static aberration ϕ_0 present in the imaging system are duly compensated for. The optimised control signals vector $\boldsymbol{\alpha^0} = [\alpha_1^0, \alpha_2^0, \ldots, \alpha_N^0]$ is recorded and used as the reference state of the MMDM in this experiment. The corresponding intensity distribution in the focal plane I_0 has the minimum second moment SM_0.

2. A reference Shack-Hartmann pattern that corresponds to the aberration free system was registered in the Shack-Hartmann sensor.

3. To measure the influence function of a single MMDM actuator with number i, we apply a control vector $\boldsymbol{\alpha^i}$ consisting of the reference control signals α^0 applied to all the actuators, except i, to which we apply the maximum control signal 0.9:

$$\boldsymbol{\alpha^i} = [\alpha_1^0, \ldots, \alpha_{i-1}^0, 1, \alpha_{i+1}^0, \ldots, \alpha_N^0]. \tag{10}$$

   We grab the corresponding Shack-Hartmann pattern, process it to find the influence function, calculate its gradient and save the results. The same procedure is repeated for all other actuators. Fig. 3 shows the measured influence function of the 19 actuators.

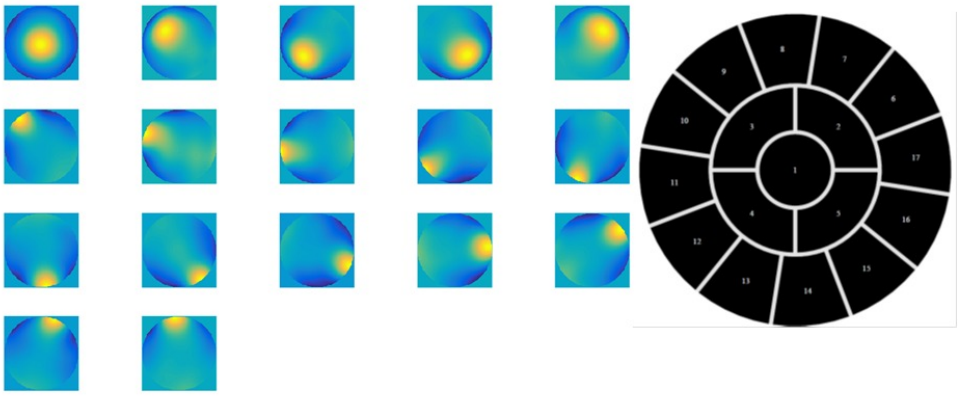

Figure 3: Experimentally measured influence functions produced by the action of each isolated actuator over the membrane of the MMDM. Position 1, 3 and 19 have been internally disabled since they correspond to the ground, tip and tilt on the digital board respectively. The membrane is mounted over the printed actuator structure shown by the side. The actuator are arranged into three circles with radii 1.81902,4.06745 and $7.5mm$.

3.3 Verification of the linear dependence of SM on MSG

Having measured the performance limits of the actuators of the MMDM, and knowing the response functions (and thus their gradients), we have performed two experiments to verify the linear relationship between the second moment of the registered intensity distribution at the focal plane and the mean square gradient of the wavefront aberration.

First verification was performed by linearly moving in the control space from point $\boldsymbol{\alpha}^0$ in a random direction and correspondingly measuring the second moment of the registered intensity distribution. In the second experiment, 500 random aberrations were generated and the relationship between the computed SM and MSG was estimated.

With a Matlab script, a random control vector $\boldsymbol{\alpha} \in [-1, 1]^N$ is generated. A control signal $\boldsymbol{\alpha}^0 + \frac{i}{\mathrm{NM}}\boldsymbol{\alpha}, \quad i = 1, \ldots, \mathrm{NM}$, where i is the measurement number of iteration and NM is the total number of measurements was

applied to the mirror and the second moment of the intensity distribution is computed using equation (2). The CCD has a dimension of $[1280X1024]$ pixels, however, to eliminate background noise, a smaller area of interest was selected by cropping the image to a size of $[380X208]$. To compute the second moment of the random aberration with optimal accuracy, the noise of the registered image is thresholded at 10 % level, the impact of noise thresholding of the image is significantly obvious as shown in Fig. 4(a). Without noise thresholding, the computed SM was erroneous and it was practically impossible to obtain a linear relationship between the SM and the MSG of the aberration. Fig. 4(b) however shows a very linear relationship between the computed SM and the MSG after implementing noise thresholding.

To further obtain maximum information from the PSF, the image intensity was automatically controlled to avoid saturation and noise. The matlab script automatically adjusted the camera exposure rate to keep the image intensity maximum at 90% of the camera maximum level. A baseline for minimum image intensity was also defined.

To compute the MSG values, first the aberration due to the randomly generated control signals and the measured influence function matrix are computed. The mean square gradient of the estimated aberration is computed in Matlab using equation (8).

The same procedure was repeated for 500 random aberrations. In this case the aberrations were not linearly increased but randomly selected. To obtain an increasing MSG and SM however, the computed MSG was sorted and indexed in order of increasing magnitude. The corresponding second moment of the indexed MSG were obtained and plotted as shown in Fig. 4(c).

To obtain accurate values of the computed SM and MSG it was essential to employ the use of accurate scaling of measurements. Therefore we converted the SM measurements to angular coordinates using the following equation

$$u, v = \frac{x}{f}, \frac{y}{f}$$

where u, v are the angular coordinates, x, y are the coordinates of the pixels and f is the focal length of the imaging lens. The measured SM is multiplied by the pixel size ($5.2\,\mu$m). To convert the MSG to appropriate units, we multiplied the estimated MSG with the wavevector κ, where $\kappa = \frac{2\pi}{\lambda}$, the obtained MSG is then divided by the square of the pupil area.

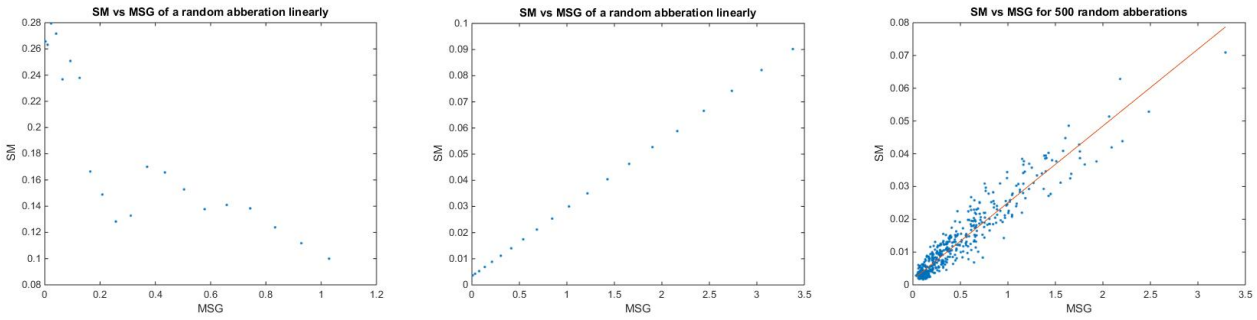

(a) Random wavefront aberrations increasing linearly without thresholding

(b) Random wavefront aberrations increasing linearly with thresholding

(c) 500 random wavefront aberrations

Figure 4: Linear dependence of the second moment of a point source on the averaged square of the phase gradients.

Relation between the MSG and the SM for a point source calculated for 500 randomly generated aberrations with various MSG are shown in Fig. 4(c). It can be seen that the mean square of wavefront gradients MSG and the second moments have an approximate linear relation. From the trend line, the value of the estimated slope c_0 is 0.0246 which is approximately equivalent to the theoretical value of $\frac{1}{4\pi^2}$. From the above figures, it is quite obvious that the experimental results are quite consistent with the simulated results obtained by Yang *et al.*[1]

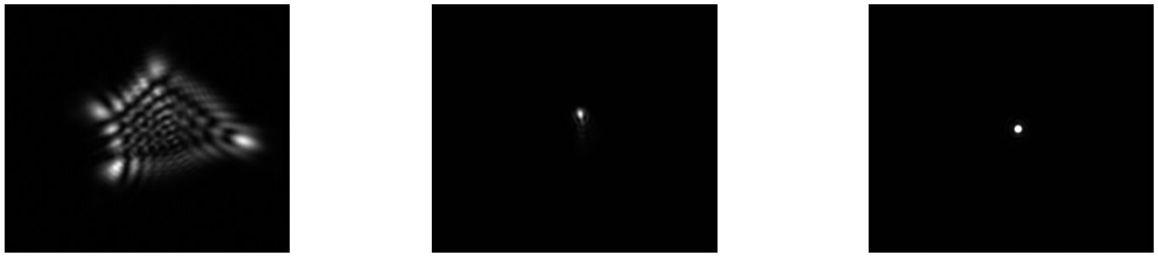

(a) Random aberration generated by the MMDM

(b) Correction without compensating for the non-common path error

(c) Correction with compensation for the non-common path error

Figure 5: Correction of the aberration introduced by the mirror

From the plot of the 500 random wavefront aberrations, an obvious deviation from trend line due to the non-common path error introduced by the path difference between the calibration arm and the focal plane can be observed. This non common path error is taking into due consideration in subsequent section.

3.4 Correction of a random aberration introduced by a mirror

To evaluate the correction capabilities and convergence of the model based algorithm, an unknown random aberration was generated by applying a vector of 17 random control signals to the actuators of the deformable mirror. The corresponding second moment (SM) of the intensity distribution of the aberration was evaluated and represented as SM_0. Next, we computed the mean square gradient of the wavefront aberration from the measured influence functions (obtained in section 3.2) according to equation (5). From the obtained mean square gradient depicted as S, inverse matrix S^{-1} , and vector S_m (diagonal vector of matrix S) were calculated once and for all.

The coefficient vector of the basis function β was computed by subtracting the optimised control signal vector $\boldsymbol{\alpha^0} = [\alpha_1^0, \alpha_2^0, \ldots, \alpha_N^0]$ obtained in section 3.2 from the maximum control signal value (0.931) obtained in section 3.1. The computed values of β were sequentially added to the random wavefront to be corrected by poking each actuator accordingly.

Correspondingly, the second moment of the intensity distribution of the superimposed aberrations were measured and M was obtained in accordance to equation (4). Using equation (3), we computed the control signal vector needed for the correction of the random aberration and applied it to the MMDM. Fig. 5(b) shows the initial correction of the random aberration shown in Fig. 5(a).

To further improve the quality of correction, we calibrated our system to compensate for the error introduced by the non-common path. We achieved this by first averaging the computed control signal vector of several iterations (one iteration is N+1 measurement where N is number of actuators). The averaged control signal vector is subtracted from the optimised control signal earlier obtained and the resultant vector is the error introduced by the non-commmon path. The computed error is added to the subsequent computed control signal vector and applied to the actuators of the MMDM. The improved result obtained is shown in Fig. 5(c).

3.5 Correction of an external aberration

To further validate the correction capabilities of the model based method, an external aberration (a transparent phase plate) was inserted at the pupil plane of the lens L_2. The telescope formed by lenses L_2 and L_3 conjugates the aberration generator to the surface of the MMDM. Following the same procedure described in the previous section but with the control signals of the actuators all set to zero, the model based algorithm was implemented and the results obtained is shown in Fig. 6.

The correction capability of the model based algorithm is also measured by the Mean Radius (MR) of the far-field intensity distribution. The MR can be calculated with equation 2. The smaller the MR value, the more

(a) External aberration generated with an aberration generator

(b) Correction with model based algorithm

Figure 6: Correction of the external aberration

focused the far field energy is and the smaller the aberration. Tabulated values of the mean radius based on the correction of both the model based approach and the conventional classical iterative optimisation methods is shown in Table 1.The MR of the model based algorithm is minimal indicating an excellent correction capabilities as compared to the SPGD, furthermore, the removal of the static error (SE) shows improved correction. It can also be inferred that the model based method produces an optimal solution with minimal convergence rate as only 20 $(N+1)$ measurements is required where N is the number of actuators.

Table 1: The final mean radius of the corrected aberration for different methods. The mean radius of initial aberration was 0.5813.

Method	Number of measurements	Final mean radius
Model-free	21	$0.51\,\mu$m
Model-based $+SE$	21	$0.0251\,\mu$m
Model-based $-SE$	21	$0.0075\,\mu$m

4. CONCLUSION

The second moment of the intensity distribution change in the focal plane is proportional to the integral of the square of the phase derivative multiplied by pupil function for the point source. The simulation results presented in their work has been experimentally validated in this paper. The Image second moment and the phase mean square gradient of wavefront aberrations have been calculated and analysed with linear regression. The experimental results validates the linear dependence of SM on MSG of the wavefront aberration for a point source. The experimental results are consistent with simulation results and theoretical estimates when effective noise thresholding is applied. The measured influence functions of the deformable mirror was used as the basis function needed for the control algorithm to make full use of the correction capability of the DM so as to obtain rapid convergence. An adaptive optics experimental imaging system with a 19 channel MMD, a CCD and Wavefront sensor has been set-up in our laboratory,and the correction capability and convergence speed of the proposed model has been experimentally investigated and compared to a a model free algorithm. The research results shows that the Model-based algorithm provides a superior performance in aberration correction in terms of capability and convergence speed as compared to the SPGD algorithm.

ACKNOWLEDGMENTS

This work is sponsored by the European Research Council, Advanced Grant Agreement No. 339681.

REFERENCES

[1] Yang, H., Soloviev, O., and Verhaegen, M., "Model-based wavefront sensorless adaptive optics system for large aberrations and extended objects," *Optics Express* **23**, 24587 (sep 2015).

[2] Vdovin, G. V., "Optimization-based operation of micromachined deformable mirrors," *Proceedings of SPIE* **3353**, 902–909 (1998).
[3] Antonello, J., "Optimisation-based wavefront sensorless adaptive optics for microscopy."
[4] Antonello, J. and Verhaegen, M., "Modal-based phase retrieval for adaptive optics," *Journal of the Optical Society of America A* **32**, 1160 (jun 2015).
[5] Booth, M., "Wave front sensor-less adaptive optics: a model-based approach using sphere packings.," *Optics express* **14**, 1339–52 (feb 2006).
[6] Delphine, D., Booth, M. J., and Wilson, T., "Image based adaptive optics through optimisation of low spatial frequencies Abstract :," **15**(13), 8176–8190 (2007).
[7] Antonello, J., van Werkhoven, T., Verhaegen, M., Truong, H. H., Keller, C. U., and Gerritsen, H. C., "Optimization-based wavefront sensorless adaptive optics for multiphoton microscopy," *J. Opt. Soc. Am. A* **31**, 1337–1347 (jun 2014).
[8] Booth, M. J., "Wavefront sensorless adaptive optics for large aberrations," *Optics Letters* **32**(1), 5 (2007).
[9] Linhai, H. and Rao, C., "Wavefront sensorless adaptive optics: a general model-based approach.," *Optics express* **19**(1), 371–379 (2011).
[10] Geng, C., Luo, W., Tan, Y., Liu, H., Mu, J., and Li, X., "Experimental demonstration of using divergence cost-function in spgd algorithm for coherent beam combining with tip/tilt control," *Opt. Express* **21**, 25045–25055 (Oct 2013).
[11] Zakynthinaki, M. and Saridakis, Y., "Stochastic optimization for a tip-tilt adaptive correcting system," *Computer Physics Communications* **150**(3), 274 – 292 (2003).